International Journal of Solids and Structures 243 (2022) 111593

Contents lists available at ScienceDirect

International Journal of Solids and Structures

journal homepage: www.elsevier.com/locate/ijsolstr

Prediction of flexural drift capacity in masonry walls through a nonlinear truss-based model

A.M. D'Altri *, S. de Miranda

Department of Civil, Chemical, Environmental, and Materials Engineering (DICAM), University of Bologna, Viale del Risorgimento 2, Bologna 40136, Italy

ARTICLE INFO

Keywords:
Pushover
Crushing
Drift
Seismic response
Masonry mechanics
Unreinforced masonry

ABSTRACT

In this paper, the in-plane flexural drift capacity of masonry walls is numerically investigated. In particular, a nonlinear truss-based model is specifically developed to predict the monotonic response of in-plane horizontally-loaded masonry walls undergoing flexural failure, so that to investigate their deformation capacity. This novel modelling strategy assumes a band of nonlinear truss elements at the wall toe to account for flexural failure. The truss elements are supposed no-tension with plastic-softening behaviour in compression. This simple and original model is easily and fully characterizable by experimentally-based compressive stress–strain relationships available in the literature for different masonry types. The modelling strategy is validated against two different pier-scale experimental tests which experienced flexural failure. The model is then used to predict the flexural drift capacity of walls with different masonry types and geometrical features, subjected to a full-range of axial load ratios. As a result, drift capacity is found to nonlinearly decrease while increasing the axial load ratio, and to be sensibly dependent on the wall width (i.e. drift capacity diminishes while increasing wall width), for any masonry type. Finally, a simple analytic expression based on numerical results is deduced for the flexural drift capacity of masonry walls, function of axial load ratio, masonry type, and wall size. Accordingly, this analytic expression could be implemented in any structural analysis masonry-oriented commercial code to account for a consistent description of the flexural drift capacity of masonry walls.

1. Introduction

The structural assessment of existing masonry buildings is typically pursued by means of numerical tools, which showed a considerable development in the last decades (D'Altri et al., 2020). Four main categories of numerical models, which attempt to deal with the complex masonry mechanics (Almeida and Lourenço, 2020; Drougkas et al., 2019; Milani and Taliercio, 2016; Cavalagli et al., 2013; Baraldi et al., 2018), can be recognized (D'Altri et al., 2020): (i) block-based models, which idealize the structure block-by-block (Nodargi et al., 2019; Lancioni et al., 2013; Smoljanović et al., 2018; Chisari et al., 2018; Serpieri et al., 2017), (ii) continuum models, which adopt equivalent homogeneous continua (Bacigalupo et al., 2021; Addessi and Sacco, 2016; Clementi et al., 2018; Di Nino and Luongo, 2019; Gatta et al., 2018; Nodargi and Bisegna, 2019), (iii) geometry-based models, where the structure is idealized as a set of rigid bodies in equilibrium (Cavalagli et al., 2016; Angelillo, 2015; Gáspár et al., 2021; Portioli et al., 2015) typically adopting no-tension relations (Tralli et al., 2020), and (iv) macroelement models (Lagomarsino et al., 2013; Chácara et al., 2019; Malomo and DeJong, 2021; Raka et al., 2015; Di Nino et al., 2017), where the structure is idealized into panel-scale structural components. In particular, macroelement models (also called equivalent frame models) are the most widely utilized tools by practitioners for the seismic assessment of masonry structures, given their computational efficiency and their easy mechanical characterization (Cattari and Magenes, 2021). The structural components (piers and spandrels) have to be identified on the structure a priori (Cattari et al., 2021), typically pursuing damage observations on actual buildings. Accordingly, the mechanical characterization of the model is governed mainly by the mechanical behaviour of the masonry pier.

The mechanical response of a masonry pier subjected to horizontal loading is generally characterized by the stiffness, strength and deformation capacity (commonly represented by the drift at near collapse, also called ultimate drift). In general, these features depend on the masonry type (which could be variegated (Zhang et al., 2017), dimensions, boundary conditions, and failure mode (Celano et al., 2021). Typically, three kinds of failure mode can be observed in masonry walls: (i) flexural, (ii) diagonal shear, and (iii) sliding failures.

* Corresponding author.
E-mail address: am.daltri@unibo.it (A.M. D'Altri).

https://doi.org/10.1016/j.ijsolstr.2022.111593
Received 29 September 2021; Received in revised form 3 March 2022; Accepted 22 March 2022
Available online 24 March 2022

On the one hand, simple analytical models exist from a long time (Turnšek and Sheppard, 1980; Turnšek and Čačovič, 1971; Mann and Müller, 1982) to estimate the strength of in-plane-loaded masonry walls, and they generally provide reliable predictions of the wall strength. On the other hand, the prediction of the deformation capacity of in-plane-loaded masonry walls results more challenging and more investigation appears to be needed (Petry and Beyer, 2015; Messali and Rots, 2018). This aspect is also reflected by national and international technical standards, which indeed suggest very simplified empirically-based laws for drift at failure of masonry walls, typically based on quasi-static cyclic experimental tests on masonry piers (Morandi et al., 2021; Rezaie et al., 2020). However, these tests are very expensive, and the range of applicable boundary conditions appears quite limited. A comprehensive review of flexural drift capacity models in international standards, guidelines and literature can be found in (Messali and Rots, 2018; Petry and Beyer, 2014). Here, it is just stressed the fact that no available drift capacity model accounts for the masonry type (i.e. the material properties of the wall). In this context, Eurocode EC8-3 (CEN, 2005) supplies an estimate of flexural drift capacity at near collapse only based on the ratio between the shear span (the distance between the height of null moment and the wall base) and the wall height, while the Italian code NTC (Technical Norms, 2018) and its commentary (Commentary, 2019) suggest an estimate of flexural drift capacity only function of the boundary conditions (cantilever or not). Only the Swiss masonry standard SIA D0237 (SIA, 266. Mauerwerk, 2015) appears to estimate the drift capacity as function of the axial load ratio (ALR), i.e. the axial stress of the panel normalized with respect to the masonry compressive strength, without however distinguishing the drift capacity between flexural or shear failure modes.

The challenging estimation of drift capacity of masonry piers is also reflected in equivalent frame models, currently used by practitioners, which generally adopt a priori constant conventional values of drift at near collapse: typically, 0.6% for flexural failure and 0.4% for shear failure, independently from the ALR (D'Altri et al., 2021). Although the ALR of masonry walls in existing buildings in static conditions is generally lower than 25% (Petry and Beyer, 2014), the ALR could significantly increase due to stress redistribution along with pushover analyses, leading the aforementioned assumption on drift at near collapse to be unsafe for high values of ALR.

An effort to address accurate predictions of the flexural drift capacity of masonry piers has been lately investigated through analytical models. An analytic formulation for the prediction of flexural drift capacity of masonry walls based on local performance limits in the compressed wall toe was developed by Benedetti & Steli (Benedetti and Steli, 2008), then extended to more general cases (in terms of shear span) by Petry & Beyer (Petry and Beyer, 2015). These models are based on the assumption of an elastic plastic material in the compressed zone with a limited compression strain, given that, in flexural failure, vertical splitting cracks appear in the bricks of the compressed toe, typically starting from the second bed joint from the bottom. An extension of the Petry & Beyer model to shear failure has been presented by Wilding & Beyer (Wilding and Beyer, 2017) through the so-called Critical Diagonal Crack model. This model has been then simplified into an equation suitable for code implementation in (Wilding and Beyer, 2018), where the predicted drift capacity agreed with test results and highlighted the influence of the ALR and dimensions on drift capacity. Although these models are elegant, they are not able to take into account the masonry properties in evaluating the drift capacity. Also, they are based on few simplistic assumptions without experimental evidence, e.g. in defining the length of the compressed zone at the wall toe in near collapse conditions.

To the best of the authors' knowledge, the only attempts to estimate the in-plane drift capacity of masonry walls through a numerical model have been carried out by Dolatshahi et al. (Dolatshahi et al., 2018), through a block-based model which implements 3D blocks and cohesive interface surface elements, and by Orlando et al. (Orlando et al., 2016), through total strain crack and a plastic models. The first approach represents an accurate solution for the simulation of quasi-static cyclic tests on masonry piers, and very interesting results can be found in (Dolatshahi et al., 2018), for both flexural and shear failures, where also the size effect is observed. However, a large number of parameters need to be known or calibrated to mechanically characterize the model (indeed, only one masonry material has been considered in (Dolatshahi et al., 2018), and these parameters could have a significant influence on the drift capacity. Also, such block-based model appears to have a nonnegligible computationally demand given the use of 3D damaging blocks with softening and cohesive interface elements, which would in general limit the use in a wide range of materials, dimensions and boundary conditions. The latter approach (Orlando et al., 2016) represents an efficient solution for the analysis of masonry panels. However, the mechanical characterization of a 2D homogeneous continuum appears not trivial. Indeed, many mechanical parameters have been tuned by the authors in (Orlando et al., 2016) to fit experimental results. In this framework, homogenization-based procedure with nonlinear interfaces could be employed to recover homogenized mechanical properties in simplified numerical approaches, see for example (Bertolesi et al., 2016; Addessi et al., 2021).

In addition, according to the authors' experience (see e.g. (D'Altri et al., 2021), the use of 2D and 3D continuum models and block-based models with nonlinear continuum laws appears nontrivial even on simple benchmarks such as masonry piers, whose response may be, indeed, significantly influenced by many factors (e.g. top warping, transverse confinement, etc.), as well as convergence and regularization issues may appear given the constitutive laws with softening. Also, the simulation of no-tension materials with crushing failure appears not trivial through this kind of models.

In this framework, this paper aims to present the simplest numerical model able to predict flexural drift capacity of masonry walls (shear failures will be investigated in future research). The simplicity of the model is a crucial aspect as a comprehensive investigation of the flexural drift capacity of walls with different masonry types, aspect ratios and global sizes subjected to a full-range of axial load ratios would require:

- a simple and easy mechanical characterization of the model, possibly based on literature data;
- a very limited computational effort of the model to guarantee a large number of numerical simulations in a reasonable amount of time;
- a robust response of the model, without algorithmic convergence/solution issues.

In this paper, the in-plane flexural drift capacity of masonry walls is investigated through a nonlinear truss-based model specifically developed to predict the monotonic response of in-plane horizontally-loaded masonry walls undergoing flexural failure. The trusses are supposed no-tension with plastic-softening behaviour in compression. Accordingly, the model appears easily mechanically characterizable by experimentally-based compressive stress–strain relationships which can be found in the literature for different masonry types. The height of the band of trusses is assumed equal to two rows of blocks, i.e. the zone in which crushing failure is typically observed (Petry and Beyer, 2015; Dolatshahi et al., 2018). The modelling strategy is validated against two different pier-scale experimental tests which experienced flexural failure. The model is then used to predict the flexural drift capacity of walls with different masonry types and geometrical features, subjected to a full-range of axial load ratios. Finally, a simple analytic expression based on numerical results is deduced for the flexural drift capacity of masonry walls.

The paper is structured as follows. Section 2 presents the modelling strategy and its validation. Section 3 shows a comprehensive numerical prediction of the drift capacity on a full-range of ALR values for several masonry types and for several masonry panel geometries. Section 4 presents an analytic expression for drift capacity based on the numerical results. Sections 5 collects the conclusions of this study.

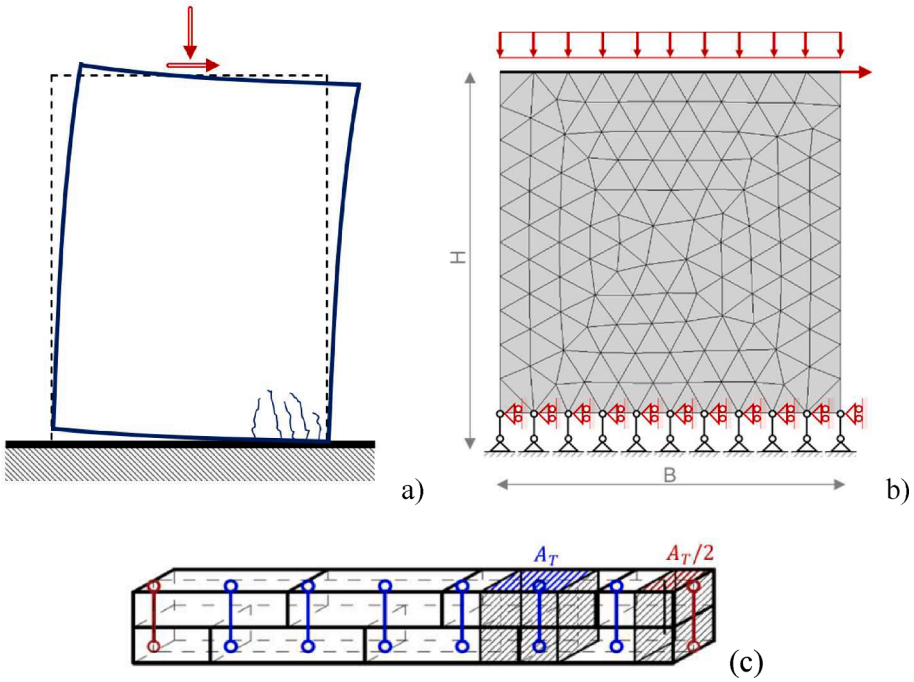

Fig. 1. Sketch of the flexural failure in a masonry wall (a) and modelling assumptions (b). Truss spacing at the wall toe (c).

2. Modelling strategy

In this section, the modelling assumptions as well as the model characterization and validation are discussed in detail.

2.1. Modelling assumptions

The modelling strategy herein proposed accounts for the in-plane flexural behaviour of masonry walls. Accordingly, all mechanical nonlinearities are lumped at the wall toe. Indeed, as it can be noted in Fig. 1(a), the flexural failure (or rocking failure) of a masonry panel subjected to vertical (compressive) and horizontal loads is typically characterized by the opening of a sub-horizontal crack in the tensile zone and the formation of a series of sub-vertical cracks in the compressive zone, i.e. crushing (De Falco and Lucchesi, 2007). Consequently, it appears reasonable to believe that most of nonlinear phenomena take place in a small wall portion in correspondence of the wall toe. Indeed, experimental outcomes point out that crushing due to flexural failure typically occur within the first two rows of blocks at the wall toe, as also considered in the analytic formulation proposed in (Petry and Beyer, 2015). It should be underlined that these considerations are valid as long as no diagonal shear cracks occur, i.e. with a dominating flexural mode failure. Indeed, this paper focuses on flexural failure only, leaving shear failure modes to future research.

According to the above considerations, a band of nonlinear trusses with vertical axis and height equal to two rows of blocks is introduced at the wall toe to account for flexural failure, while the rest of the panel is modelled with a linear elastic continuum (Fig. 1(b)).

The idea at the base of this modelling strategy comes from the traditional solution for flexural failure in masonry panels, in which a lumped-plasticity hinge is supposed at the wall toe, considering a no-tension response and a compressive stress-block with infinite plastic deformations. In the modelling strategy herein proposed, a sort of finite-thickness hinge with plastic-damaging response is somehow supposed through the use of nonlinear vertical truss elements to investigate the flexural drift capacity of masonry walls.

In this model, 2D standard 2-node linear displacement truss elements are considered for the trusses, and 2D standard 3-node linear displacement plane stress elements are considered for the continuum. The truss spacing is here assumed so that each truss represents half block in the horizontal direction, i.e. the truss area A_T is equal to the area of the top surface of half block. As highlighted in Fig. 1(c), truss elements with halved area $A_T/2$ are considered at the wall lateral extremities to guarantee constant spacing of the trusses and avoid free corners. As highlighted by preliminary analyses, the truss spacing and the use of truss elements with halved area at the extremities has not been found to have a significant influence on the structural response. Nonetheless, the truss spacing herein adopted appears reasonable as it represents the minimum periodic dimension in common masonry textures.

The linear elastic behaviour of the continuum could be assumed isotropic or orthotropic. In this case, an isotropic continuum is assumed, for simplicity, following the calibration of the elastic moduli of masonry walls proposed in (D'Altri et al., 2021). The nonlinear constitutive model for the truss elements is discussed in the following subsection.

Concerning the boundary conditions, vertical and horizontal displacements are constrained at the lower extremity of the truss elements, while only horizontal displacements are constrained at their upper extremity (Fig. 1(b)). These conditions, which are substantially equivalent to subtract the shear deformability of two rows of blocks, has not been found to significantly influence the structural response in common wall dimensions. Accordingly, such an assumption enforces a uniaxial vertical stress state at the wall toe, which is indeed strategical in investigating the flexural response.

The wall top edge is constrained through a master–slave kinematic condition equivalent to a rigid body, as commonly pursued to account for the presence of stiff ring beams on the top of masonry piers (D'Altri et al., 2021). Imposed horizontal displacement is applied on the master node, while vertical (compressive) distributed load is applied uniformly on the top edge.

2.1.1. Truss nonlinear constitutive model

Truss elements are supposed no-tension with plastic-softening behaviour in compression. Limiting the discussion here to the compressive regime, the compressive strain ε_c is decomposed into the elastic part ε_c^e and the plastic part ε_c^p as in the incremental theory of plasticity:

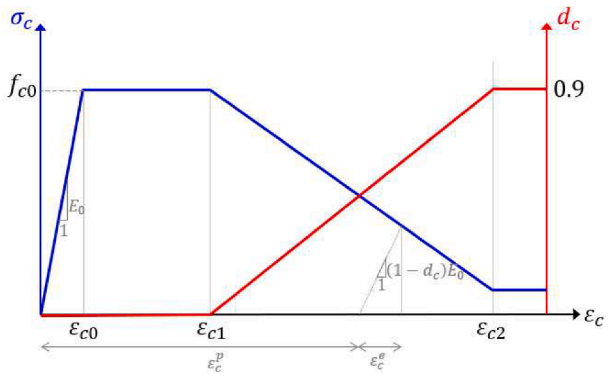

Fig. 2. Example of a simplified trilinear compressive stress–strain relationship (blue curve) together with compressive damage evolution (red curve).

$$\varepsilon_c = \varepsilon_c^e + \varepsilon_c^p. \tag{1}$$

The compressive stress σ_c (assumed positive in compression) is related to the effective compressive stress $\overline{\sigma}_c$ through the standard scalar degradation relation:

$$\sigma_c = (1 - d_c)\overline{\sigma}_c, \tag{2}$$

where d_c is the compressive scalar damage variable, dependent on the accumulated compressive plastic strain, i.e. $d_c = d_c(\varepsilon_c^p)$. The scalar d_c can vary from 0 (undamaged) to 1 (fully damaged), and it is a non-decreasing quantity, i.e. the damage rate is $\dot{d}_c \geq 0$.

Here, the plasticity problem is conveniently formulated in terms of the effective stress (Lee and Fenves, 1998):

$$\overline{\sigma}_c = E_0(\varepsilon_c - \varepsilon_c^p), \tag{3}$$

being E_0 the initial Young's modulus of the truss. The compressive stress σ_c is then expressed, using (2) and (3), as:

$$\sigma_c = (1 - d_c)E_0(\varepsilon_c - \varepsilon_c^p). \tag{4}$$

Taking into account (1), from (4) it follows:

$$\varepsilon_c^p = \varepsilon_c - \varepsilon_c^e, \qquad \varepsilon_c^e = \frac{1}{1 - d_c}\frac{\sigma_c}{E_0}. \tag{5}$$

The plasticity problem is described by a yield function $F_c = F_c(\overline{\sigma}_c, \varepsilon_c^p)$, which is assumed to have the form:

$$F_c = \overline{\sigma}_c - \overline{f}_c(\varepsilon_c^p), \tag{6}$$

being $\overline{f}_c(\varepsilon_c^p)$ the yield stress under compression in effective stress, with $f_c = (1 - d_c)\overline{f}_c$ the compressive yield stress, and by a flow rule:

$$\dot{\varepsilon}_c^p = \dot{\lambda}\frac{\partial F_c}{\partial \overline{\sigma}_c}, \tag{7}$$

being $\dot{\lambda}$ the rate of the plastic multiplier, as well as the plastic consistency condition:

$$F_c \leq 0, \quad \dot{\lambda} \geq 0, \quad \dot{\lambda}F_c = 0. \tag{8}$$

It should be pointed out that the functions $d_c = d_c(\varepsilon_c^p)$ and $f_c = f_c(\varepsilon_c^p)$ represent the only input of the present constitutive model, and they are function of the accumulated compressive plastic strain. In this research, the functions $d_c = d_c(\varepsilon_c^p)$ and $f_c = f_c(\varepsilon_c^p)$ are specified pointwise.

Also, it should be noted that in (5) both $(1 - d_c)$ and σ_c tend to zero for fully damaged materials, given that the maximum actual value of σ_c, i.e. f_c, tends to zero for a damaged material. Non-zero residual values may be then adopted for $(1 - d_c)$ and f_c to guarantee convergence in the softening regime. Accordingly, d_c is herein limited to 0.9 while f_c is assumed to be not lower than $10\%f_{c0}$. This simplification does not appear to significantly influence the structural response, as highlighted in Appendix A where the compressive damage upper limit and the residual stress have been varied in the range 0.85 ÷ 0.99 and $15\%f_{c0}$ ÷ $1\%f_{c0}$, respectively.

In Fig. 2, an example of a simplified trilinear compressive stress–strain relationship is shown together with the compressive damage evolution (where the compressive strength is denoted with f_{c0}). Particularly, the quantity ε_{c0} refers to the compressive strain at the linear elastic limit, i.e. $\varepsilon_{c0} = f_{c0}/E_0$, ε_{c1} indicates the compressive strain at the end of the plateau, while ε_{c2} is the compressive strain at the end of the softening branch. Beyond ε_{c2}, compressive damage and stress remain constant and equal to the residual values.

The tensile response of truss elements is supposed to be no-tension. Accordingly, the same above considerations for the compressive regime are valid also in the tensile regime, although dummy and very low tensile strength (e.g. 1 Pa) and ultimate deformation values are adopted to practically simulate a no-tension response. It should be noted that this assumption appears particularly worthy in truss elements (uniaxial behaviour) and is not suggested, e.g., for 2D or 3D continuum finite elements to guarantee convergence and stability.

Finally, it should be highlighted that once one truss element experiences tensile strain in its loading history, it is assumed to be unable to sustain any possible compressive stress in the following increments, i.e. no stiffness recovery is herein considered. This assumption appears reasonable as the model aims at predicting the in-plane flexural drift capacity of masonry walls subjected to monotonic horizontal loads.

Furthermore, it is pointed out that the truss elements at the wall toe are not further discretized, and so no regularization issues of the softening behaviour can arise. This constitutive model is integrated in the Abaqus software (Abaqus, 2019) adopting the backward Euler method, also using a material Jacobian consistent with this integration operator for the equilibrium iterations.

2.2. Model characterization

From Section 2.1 it appears clear that the only aspect that needs to be mechanically characterized in the present modelling strategy is the compressive behaviour of masonry. Typically, the failure and post-failure masonry compressive responses are experimentally measured through compression tests on masonry wallets (Jafari et al., 2019; CEN, 2002). It should be herein underlined that these tests have been widely adopted for several masonry types, and indeed several stress–strain relationships for masonry under compression have been lately proposed (Kaushik et al., 2007; Augenti and Parisi, 2010).

In compressive tests on masonry wallets, vertical deformations are typically measured through linear variable differential transformers (LVDTs), which measure variations of vertical displacement. Accordingly, the potential outcome of these tests could be represented by both stress-displacement and stress–strain curves, where the passage from the first to the second can be easily conducted by subdividing the first by the initial LVDTs length. It is herein pointed out that the area underneath the whole stress-displacement curve can be considered as the compressive fracture energy (Jafari et al., 2019). Nonetheless, the experimental scientific community generally employs and discusses stress–strain curves (Kaushik et al., 2007; Augenti and Parisi, 2010), and the fracture energy is evaluated in a few cases only (Jafari et al., 2019).

In this modelling strategy, the stress–strain curves obtained in experimental tests (and/or the ones deduced from experimentations) are directly employed in the nonlinear truss elements described in Section 2.1.1. Accordingly, the resulting compressive fracture energy of a truss element consists in the area underneath the stress–strain curve times the length of the truss element (l_T), which is here assumed to be equal to the height of two rows of blocks. This assumption appears reasonable as:

(i) In experimental campaigns, the initial LVDTs length is generally rather close to the height of two rows of blocks, as can be also deduced from the reference testing protocol (Cen, 1998).

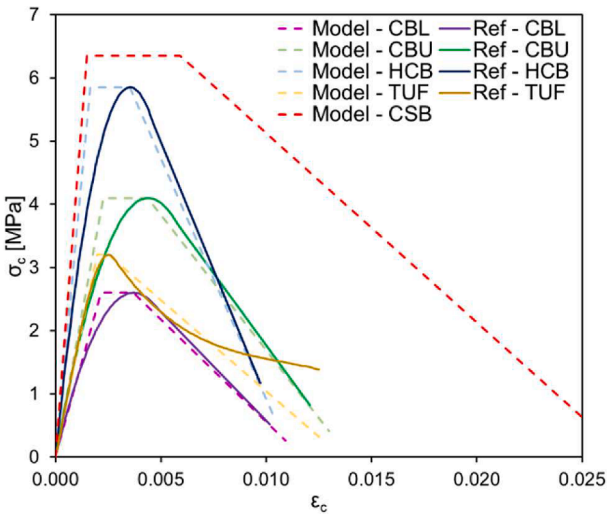

Fig. 3. Compressive stress–strain relationships for the masonry types considered. "Ref" refers to the reference curve, "Model" refers to the curve implemented in the numerical analyses.

Table 1
Parameters adopted to define the compressive stress–strain curves implemented in the numerical model for the five considered masonry types.

Masonry type	E_0 [MPa]	f_{c0} [MPa]	ε_{c1} [‰]	ε_{c2} [‰]
CBL	1200	2.60	3.70	10.9
CBU	1800	4.10	4.39	12.9
HCB	3550	5.85	3.53	10.4
TUF	1620	3.20	2.50	12.5
CSB	4265	6.35	5.90	25.0

Accordingly, stress–strain curves available in literature (which do not directly specify any value of fracture energy) approximately imply the compressive fracture energy herein considered.

(ii) The damaging process in flexural failure of masonry walls is typically localized in a small portion at the wall toe which can be considered akin to the initial LVDTs length generally considered in experimental tests on masonry wallets, and akin to the height of two rows of blocks (Petry and Beyer, 2015).

The experimental stress–strain curves are employed in truss elements through a trilinear response approximation (see Fig. 2), for simplicity. It should be highlighted that this simplification has not significant effects on the structural response of a wall. Indeed, preliminary analyses highlighted the substantially negligible influence on the pushover curve of assuming a quadrilinear compressive stress–strain curve with hardening rather than the trilinear curve here considered. The assumption of a compressive trilinear response allows to fully characterize the truss response by means of only 4 quantities:

I. The initial Young's modulus of the truss (E_0)
II. The compressive strength (f_{c0})
III. The compressive strain at the end of the plateau (ε_c^1)
IV. The compressive strain at the end of the softening branch (ε_c^2)

This simplification guaranties a very simple mechanical characterization with an acceptable level of reliability.

2.2.1. Considered masonry types

Here, five different masonry material types are considered, and their description and mechanical characterization are discussed. The analytical models developed by Kaushik et al. (Kaushik et al., 2007) and Augenti & Parisi (Augenti and Parisi, 2010) are considered for clay and tuff masonry, respectively, while the experimental results obtained by Jafari et al. (Jafari et al., 2019; Jafari et al., 2019) are considered for calcium silicate masonry. Particularly, reference to the Italian code (Commentary, 2019; Technical Norms, 2018) is also made to consider reference global mechanical properties of existing masonries (see Table C8.5.1 in (Commentary, 2019). The five masonry materials herein considered are:

- CBL: clay brick masonry (lower bound)
- CBU: clay brick masonry (upper bound)
- HCB: hollow clay brick masonry
- TUF: tuff masonry
- CSB: calcium silicate brick masonry

On the one hand, lower and upper bounds of clay brick masonry, i.e. CBL and CBU respectively, are deduced from the bounds of the range of mechanical properties suggested in (Commentary, 2019) for existing clay brick masonry, while adopting the stress–strain relationships from (Kaushik et al., 2007). The length of the truss elements (l_T) has been set, according to Section 2.1, equal to 0.12 m for both CBL and CBU. Mechanical properties for HCB are taken in agreement with (Petry and Beyer, 2014), while adopting the stress–strain relationships from (Kaushik et al., 2007) and l_T equal to 0.39 m. Tuff masonry (TUF) is characterized by assuming as Young's modulus and compressive strength the values suggested in the Italian code (Commentary, 2019) (regular texture, upper bound), while adopting the stress–strain relationships from (Augenti and Parisi, 2010) and l_T equal to 0.39 m. Reference to these stress–strain relationships ("Ref" curves in Fig. 3) has been made to deduce simplified trilinear stress–strain relationships to be implemented in the model ("Model" curves in Fig. 3). As can be noted in Fig. 3, the trilinear curves reasonably approximate the reference curves. This is also highlighted by the fact that the area underneath "Ref" and "Model" curves (which represent the compressive fracture energy density) does not significantly differ.

On the other hand, reference to the experimental campaigns carried out by Jafari et al. (Jafari et al., 2019; Jafari et al., 2019), which assessed also the compressive fracture energy of the material, is made to characterize CSB. Particularly, the Young's modulus and compressive strength values are assumed in agreement with (Jafari et al., 2019), while the simplified trilinear stress–strain curve has been set so that to obtain an average value of compressive fracture energy (which ranges approximately between 10 and 20 N/mm (Jafari et al., 2019; Jafari et al., 2019), i.e. 15 N/mm (considering in this case $l_T = 0.152$ m). In particular, the compressive strain at the end of the plateau (ε_{c1}) has been herein assumed equal to the value of peak strain recorded for CSB in (Jafari et al., 2019), i.e. 0.59% (Fig. 3). According to (Jafari et al., 2019), the compressive fracture energy has been calculated as the area underneath the stress-axial displacement curve measured over the height of the element, i.e. it is equal to the area underneath the compressive stress–strain curve times l_T. In particular, the compressive fracture energy G_c is here computed as:

$$G_c = l_T \int_0^{\varepsilon_{c2}} \sigma_c \mathrm{d}\varepsilon_c \tag{9}$$

The parameters adopted to define the compressive stress–strain curves implemented in the numerical model are collected in Table 1 for the five considered masonry types.

2.3. Model validation

In this section, the modelling strategy is validated against two different pier-scale experimental tests which experienced flexural failure.

2.3.1. Hollow clay brick masonry wall

The wall PUP3 of the experimental campaign carried out at the École

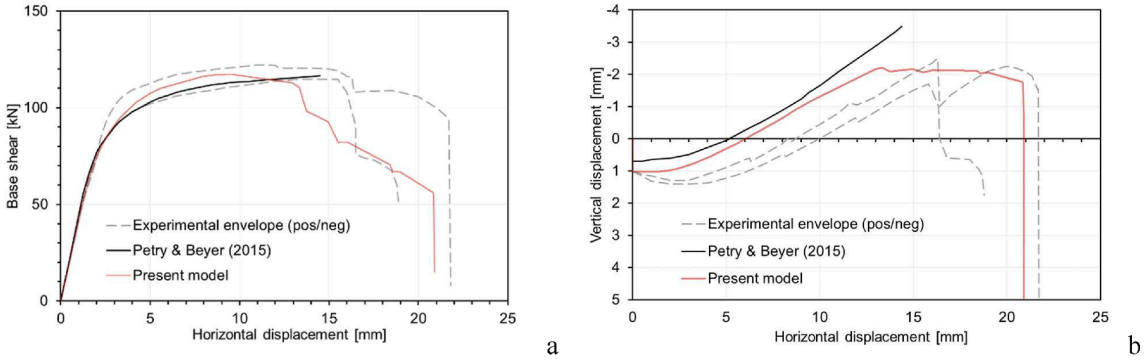

Fig. 4. Hollow clay brick masonry wall experimental–numerical validation: (a) force–displacement curves comparison, and (b) vertical-horizontal displacement curves comparison. The analytical results of Petry & Beyer (Petry and Beyer, 2015) are also reported for the sake of comparison.

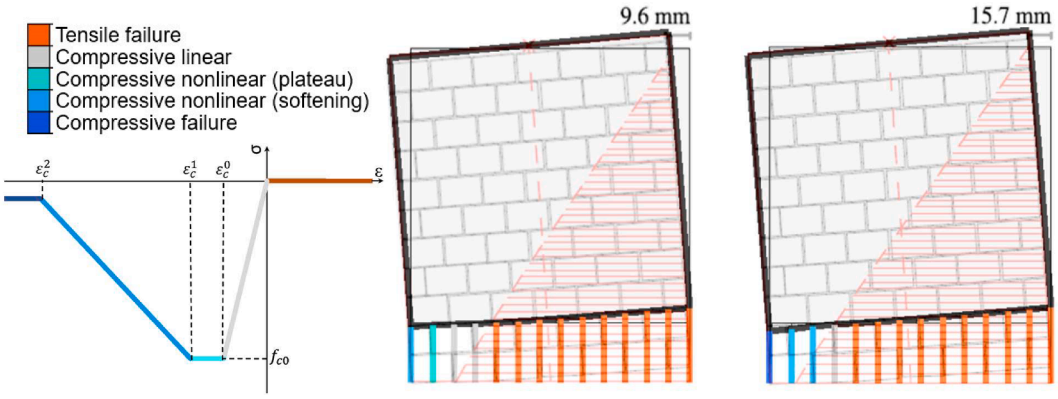

Fig. 5. Hollow clay brick masonry wall experimental–numerical validation: damaged pattern of the present model superimposed on experimental measurements (grey blocks) and analytical predictions (red lines) from (Petry and Beyer, 2015).

Polytechnique Fédérale de Lausanne (Petry and Beyer, 2015; Petry and Beyer, 2014; Petry and Beyer, 2015), which developed a typical flexural rocking failure mode, is herein considered as reference. The wall was constructed with hollow clay bricks and standard cement mortar and had dimensions of H × B × t = 2.25 × 2.01 × 0.20 m. The wall was subjected to an axial load of 419 kN (corresponding to an ALR equal to 18%) and to cyclic shear through a constant shear span of 1.5 times the wall height.

Such wall has been modelled through the numerical modelling strategy herein proposed, adopting the mechanical properties of the HCB case (see Fig. 3 and Table 1) which were taken in agreement with (Petry and Beyer, 2015). In particular, the truss length resulted to be $l_T = 0.4$ m and the linear elastic continuum has been characterized, in agreement with (Petry and Beyer, 2015), by a shear modulus equal to 890 MPa and by a Poisson's coefficient equal to 0.2.

The comparison of experimental–numerical results is shown in Fig. 4, in terms of force–displacement curves (Fig. 4a) and vertical-horizontal displacement curves (Fig. 4b, vertical displacement is assumed positive downward). Fig. 4 shows that the force–displacement and the vertical-horizontal displacement curves are well-predicted by the present model. Indeed, both peak base shear and horizontal displacement at collapse appear included within the experimental envelope (displayed for both positive and negative directions, as the shear was cyclically applied in the experiments (Petry and Beyer, 2015), although the load drop is slightly anticipated by the present model. The capability of the present model to simulate flexural failure, up to complete collapse of the masonry wall, is clearly showed by the strong softening of the force–displacement curve (Fig. 4a) and by the vertical displacement which drops sharply (Fig. 4b), as also experimentally observed. Of course, the softening of the force–displacement curve is due to the damaging of the compressed truss elements (see e.g. Fig. 5), i.e. linked to the decrement of the resisting moment they can exert when damaged.

The good predictions of the present model are also highlighted by the experimental–numerical comparison of the damage pattern, see Fig. 5 for two subsequent instants of the test (9.6 and 15.7 mm of horizontal displacement). Indeed, the deformed shapes of the present model appear in good agreement with the experimental crack patterns, hence confirming the reliability of the modelling assumptions, e.g. the band of nonlinear trusses at the wall toe. The damage pattern of the trusses appears also in line with the analytical predictions of Petry & Beyer (Petry and Beyer, 2015), i.e. tractions (red lines for the analytical predictions) are observed in mostly the same locations.

2.3.2. *Calcium silicate brick masonry wall*

The wall TUD-COMP-20 of the experimental campaign carried out at the Delft University of Technology (Messali et al., 2020), which showed a typical flexural failure mode, is herein considered as reference. The wall was built with solid calcium silicate bricks and general-purpose mortar and had dimensions of H × B × t = 2.76 × 1.1 × 0.102 m. The wall was subjected to a vertical precompression of 0.63 MPa (corresponding to an ALR equal to 10%) and to cyclic shear with cantilever boundary conditions.

The wall TUD-COMP-20 has been modelled through the numerical modelling strategy herein proposed, adopting the mechanical properties of the CSB case (see Fig. 3 and Table 1) which were taken in agreement with Jafari et al. (Jafari et al., 2019; Jafari et al., 2019). In particular, the truss length resulted to be $l_T = 0.152$ m and the linear elastic continuum has been characterized, in agreement with (Jafari et al., 2019; Jafari et al., 2019), by a Young's modulus equal to 4256 MPa and by a

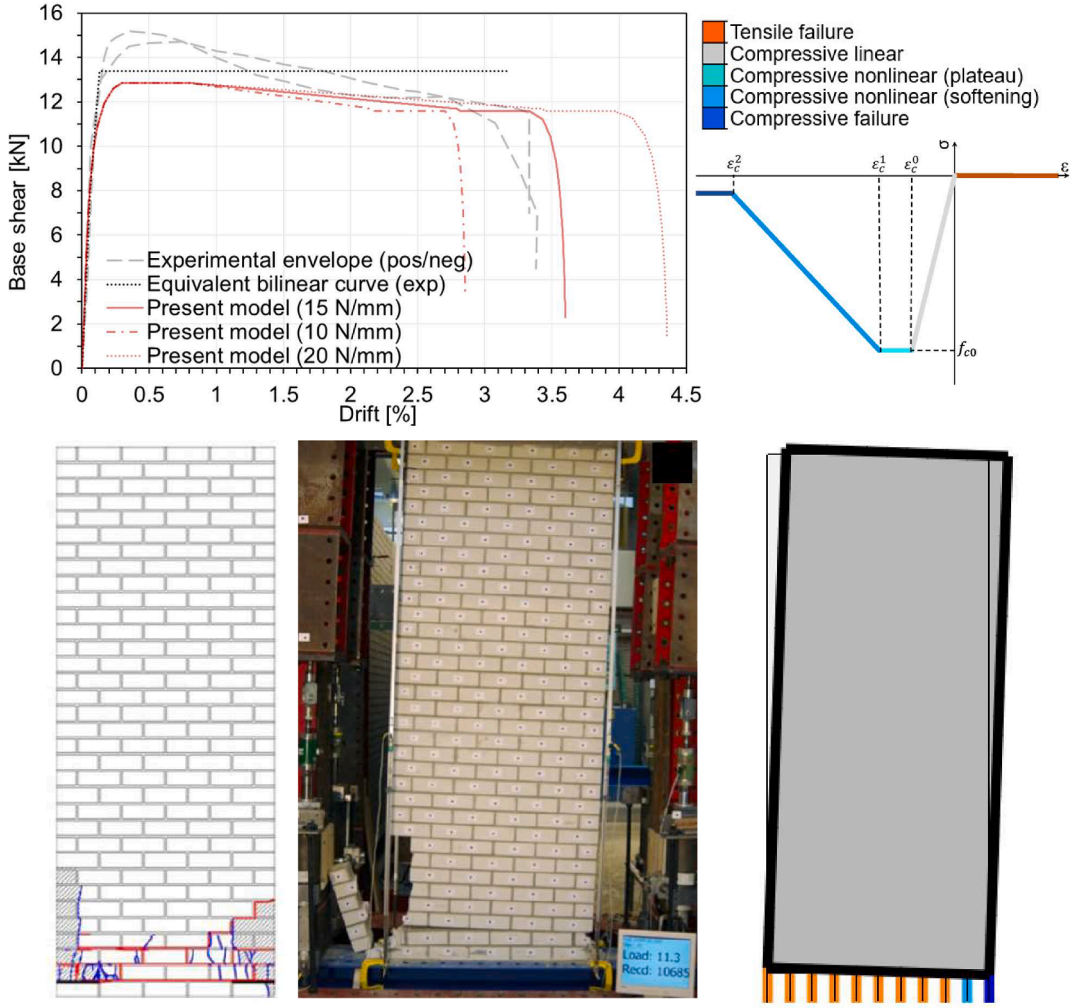

Fig. 6. Calcium silicate brick masonry wall experimental–numerical validation: force–displacement curves comparison (top left), and damaged pattern comparison (bottom), experimental pictures from (Messali et al., 2020).

Poisson's coefficient equal to 0.2. Typically, compressive fracture energy values present a high variability and a low reproducibility. This has been observed also in the experimental campaigns on calcium silicate brick masonry (Jafari et al., 2019; Jafari et al., 2019), in which the compressive fracture energy varies approximately between 10 and 20 N/mm. Accordingly, an average value equal to 15 N/mm has been assumed in the simulations.

The comparison of experimental–numerical results is shown in Fig. 6, in terms of force–displacement curves (top left) and damage pattern (bottom). In particular, beyond the numerical curve with an average value of compressive fracture energy equal to 15 N/mm, the curves obtained with 10 and 20 N/mm are also reported in Fig. 6 to show the influence of the compressive fracture energy on force–displacement curves. As expected, compressive fracture energy has not significant influence on the peak base shear load, which appears the same for the three red curves in Fig. 6, while it has a significant influence on the drift (computed here as the ratio between horizontal displacement and the height of the panel) at collapse, which increases by increasing the value of compressive fracture energy. The numerical force–displacement curve with an average value of compressive fracture energy (15 N/mm) appears in a reasonable agreement with the experimental curves (positive and negative as the shear was applied cyclically in the experiment), and with the equivalent bilinear curve extracted in (Messali et al., 2020) from the experimental results, although the peak base shear load is slightly underestimated (the model implements a no-tension response). Also in this case, the capability of the present model to simulate flexural failure up to complete collapse of the wall is clearly demonstrated by the significant drop of the base shear.

The experimental test has been conducted by applying cyclic shear to the wall, and this of course produces a crack pattern characterized by crushing at both wall toe lateral extremities (Fig. 6, bottom left). Indeed, splitting cracks in the blocks with material expulsion occurred experimentally at large drifts (Messali et al., 2020), determining a progressive origin of vertical cracks towards the wall central axis. Having this in mind, the deformed shape and the damage pattern of the present model appear in a reasonable agreement with the experimental crack ones, i.e. crushing concerns an area of approximately one block at the wall toe lateral extremity. Thereby, the hypothesis of a band of nonlinear trusses at the wall toe appeared suitable also in this case.

3. Numerical prediction of drift capacity

In this section, the nonlinear truss-based model is comprehensively exploited to predict flexural drift capacity on a full-range of ALR values for several masonry types and for several masonry panel geometries. For simplicity, flexural failure-dominated cantilever walls are the focus of this study, although akin considerations could be made on flexural failure-dominated guided-fixed walls. In all cases, geometries and boundary conditions are chosen so that the dominating failure mode is flexural, preventing shear failures.

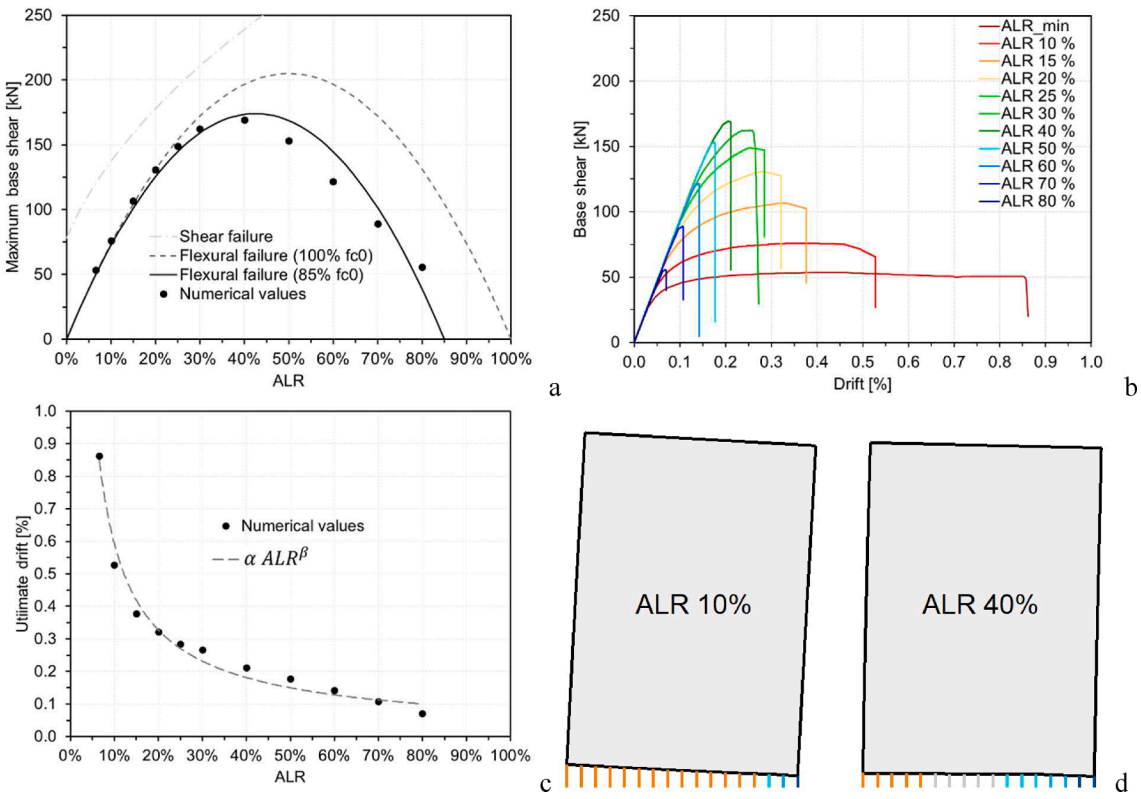

Fig. 7. Typical outcomes of the nonlinear truss-based model (material CBU, wall dimensions 3x2 m): (a) maximum base shear compared with analytical strength domains, (b) base shear-drift curves, (c) ultimate drift for the range of ALR values, and (d) damage patterns and deformed shapes at failure for ALR 10% and ALR 40%.

In this study, the drift δ is computed as the ratio between the wall top horizontal displacement and the wall height. Indeed, although several drift definitions can be used (CNR DT 212/2013), also inspired by reinforced concrete frame literature, the drift definition is herein adopted in agreement to the referenced experimental campaigns (Petry and Beyer, 2014; Messali et al., 2020).

Hereinafter, the term ultimate drift δ_u refers to flexural drift capacity of the masonry wall at near collapse, and it is defined as the drift corresponding to a force degradation equal to 20% of the maximum base shear, in agreement with existing literature (Petry and Beyer, 2014; Messali et al., 2020).

The ALR values here considered range from 5% to 80%, and more precisely the following ALR values have been considered: 5%, 10%, 15%, 20%, 25%, 30%, 40%, 50%, 60%, 70%, 80%. In particular, among the above values, only the ones resulting greater than or equal to a minimum value, i.e. ALR_{min}, are used in the numerical tests. In particular, ALR_{min} is defined as the minimum value of axial load ratio needed to reach compressive failure in a single truss element (and anyhow greater than the ALR generated by dead load of the wall), are considered. Of course, this assumption depends on the hypothesis made on the truss spacing, which is here assumed so that each truss represents half block in the horizontal direction. Indeed, denser truss spacing would have led to lower ALR_{min} values. However, the assumption here adopted on the truss spacing (half block) appears reasonable as it represents, beyond the minimum periodic dimension in masonry textures, also the minimum physical component which can exhibit crushing in a phenomenological sense. Indeed, if vertical cracks appear in half block (or in a portion of it), it is reasonable to believe that the full component (half block) has undergone failure, as more detailed consideration would be very dependent on imperfections/defects of the masonry texture. Accordingly, pushover tests on masonry walls with ALR values lower than ALR_{min} would not produce any failure in the truss elements and the wall failure would occur through the overturning of the wall, whose evaluation is out of the scope of this study.

3.1. Masonry type

In this subsection, a $H \times B = 3 \times 2$ m cantilever masonry wall is considered, and its drift capacity is evaluated for the five masonry types described in Section 2.2.1, considering a constant thickness of 0.3 m. For each material, the aforementioned range of ALR values is considered.

By way of example, the typical outcomes of the nonlinear truss-based model are collected in Fig. 7 for the material CBU. In particular, Fig. 7a shows for the various ALRs the comparison between the maximum base shear obtained numerically and analytical strength domains typically considered in the literature and codes, see e.g. (D'Altri et al., 2021). As it can be noted, the numerical values are in good agreement with the flexural strength domain with $85\%f_{c0}$, i.e. with the stress block hypothesis (D'Altri et al., 2021). Hence, for this case the fact of considering softening in the compressive behaviour matches the strength domain with stress block, whereas a perfect elastic–plastic compressive response would have been closer to the strength domain with $100\%f_{c0}$. In Fig. 7a, the shear failure strength domain (Turnšek and Sheppard, 1980) is also reported (using $\tau_0 = 0.13$ MPa in agreement with (Commentary, 2019) to highlight that the problem is flexural failure-dominated.

The base shear-drift curves obtained numerically are shown in Fig. 7b, where it can be clearly noted that the drift linked to a load drop decreases while increasing the ALR. In other words, the flexural failure becomes less ductile while increasing the ALR. This aspect is further highlighted in Fig. 7c, where the ultimate drift is plotted as function of the ALR. As it can be observed, the relationship between ultimate drift δ_u and ALR results highly nonlinear and appears reasonably approximated by the function:

$$\delta_u = \alpha \mathrm{ALR}^{\beta} \quad \text{with} \quad \alpha > 0,\ \beta < 0 \tag{10}$$

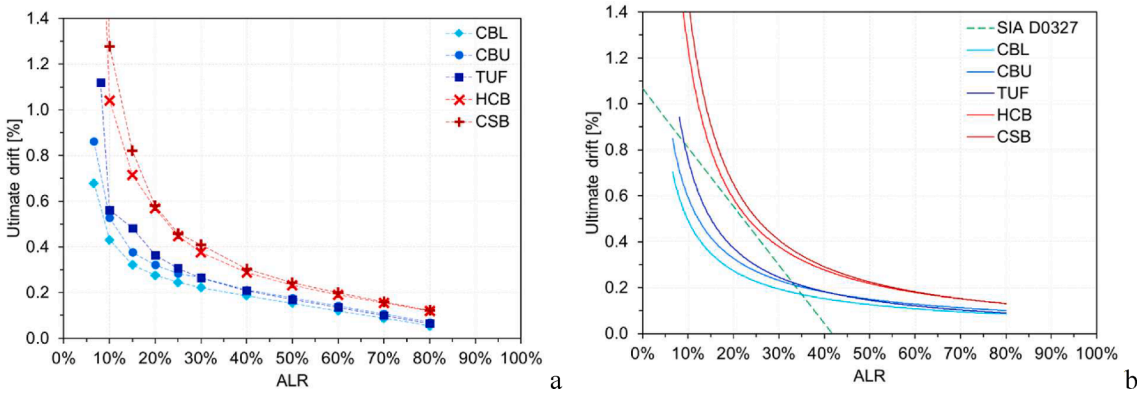

Fig. 8. Influence of the masonry type on the ultimate drift-ALR relationships (for wall dimensions 3x2 m): (a) numerical results and (b) numerically-based approximating curves (compared with the Swiss code SIA D0327 (SIA, 2015).

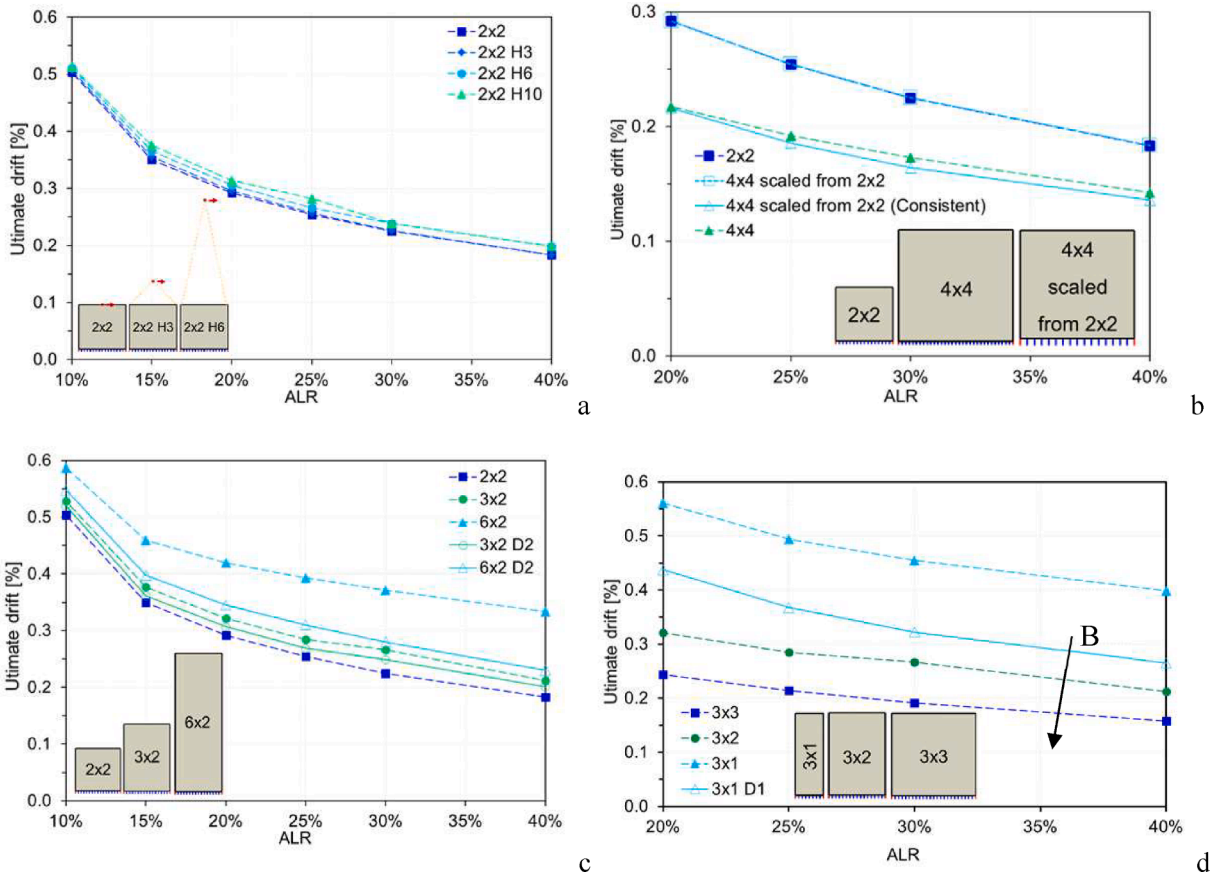

Fig. 9. Effects of geometrical features on flexural drift capacity (material CBU): (a) influence of shear span, (b) size effect, (c) influence of wall height and (d) influence of wall width.

being α and β parameters which can be obtained by standard regression procedures, and, in general, they depend on the material type and the wall dimensions.

Finally, Fig. 7d shows damage patterns and deformed shapes at failure for the cases ALR 10% and ALR 40%. As it can be noted, the two flexural failure modes show significant differences in the number of truss elements which exhibited compressive failure, as expected, thus limiting the ductility of ALR 40% with respect to ALR 10%.

It should be herein pointed out that the numerical strategy resulted very efficient from a computational point of view. Indeed, each analysis shown in Fig. 7b lasted between 30 s and 50 s on a standard commercial laptop.

Following the same workflow just presented, the ultimate drift as function of ALR has been computed for the five masonry types considered, see Fig. 8. In particular, the numerical outcomes of the ultimate drift-ALR relationships are shown in Fig. 8a, while the numerically-based approximating functions obtained by regression are shown in Fig. 8b, where they are also compared with the recommendations of the Swiss code SIA D0327 ("SIA, SIA 266. Mauerwerk., 2015), that is one of the few codes which considers the dependency (linear) of the ultimate drift on the ALR, i.e. $\delta_{u,SIA} = 4/3[0.8\%(1 - 2.4\mathrm{ALR})]$. As it can be noted, all the masonry types show the same trend and all of them appear reasonably approximated by Eq. (10). Furthermore, two response types can be observed from the responses in Fig. 8. Indeed, a first response

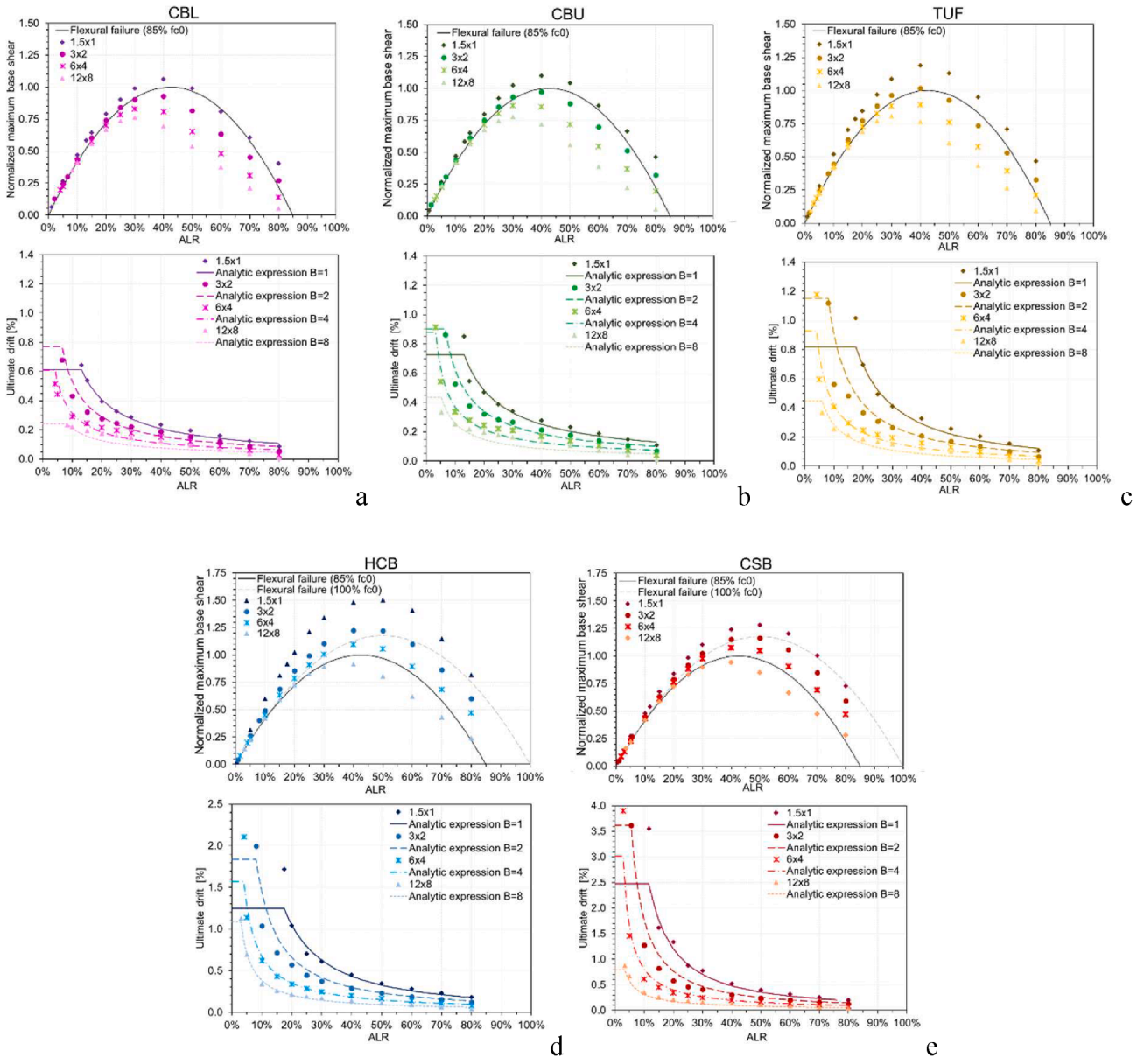

Fig. 10. Normalized maximum base shear compared with analytical strength domains (top) and numerical ultimate drift values together with analytic predictions (bottom) for a number of masonry wall dimensions: (a) CBL, (b) CBU, (c) TUF, (d) HCB, and (e) CSB material types.

Table 2
Parameters of the analytic expression for the five material types considered.

Masonry type	α_1	α_2	β_1	β_2	β_2
CBL	−0.0230	−0.0865	−0.0090	0.1131	−1.0675
CBU	−0.0310	0.1052	−0.0094	0.1054	−1.0465
TUF	−0.0260	0.0923	−0.0180	0.2160	−1.4493
HCB	−0.0410	0.1355	−0.0146	0.1868	−1.4458
CSB	−0.0470	0.1425	−0.0087	0.1466	−1.4675

type can be recognized with CBL, CBU, and TUF which show similar results in terms of ultimate drift-ALR relationships, while showing a consistent gap with another response type, composed of HCB and CSB which in turn show similar results between them. This gap appears interesting as the first response type (CBL, CBU, TUF) can coarsely represent the materials in existing masonry structures, while the second response type (HCB and CSB) can coarsely represent materials in new structures. Accordingly, a significant gap in the ultimate drift-ALR relationships can be observed between existing and new materials. Finally, it should be pointed out that, for this case, the Swiss code SIA D0327 ("SIA, SIA 266. Mauerwerk., 2015) appears to safely predict the ultimate drift for new materials (Fig. 8b), while it can overestimate the ultimate drift for existing materials.

3.2. *Geometrical features: Shear span, size effect, and aspect ratio*

In this subsection, the effects of the geometrical features in terms of shear span, size effect and aspect ratio of the wall are investigated (Fig. 9).

Firstly, the influence of shear span on the ultimate drift of masonry panels is analysed (Fig. 9a). In particular, the material CBU and square panels 2x2 m are considered. In the present case, the shear span is modified by moving the point of application of the horizontal load (through a master–slave kinematic constrain), so that to change the bending moment distribution along with the panel axis (Fig. 9a). As can be noted in Fig. 9a for a 2x2 wall, the shear span appears to not significantly influence the ultimate drift by passing from a shear span of 2 m (standard for this study) to a shear span of 3, 6, and 10 m (H3, H6

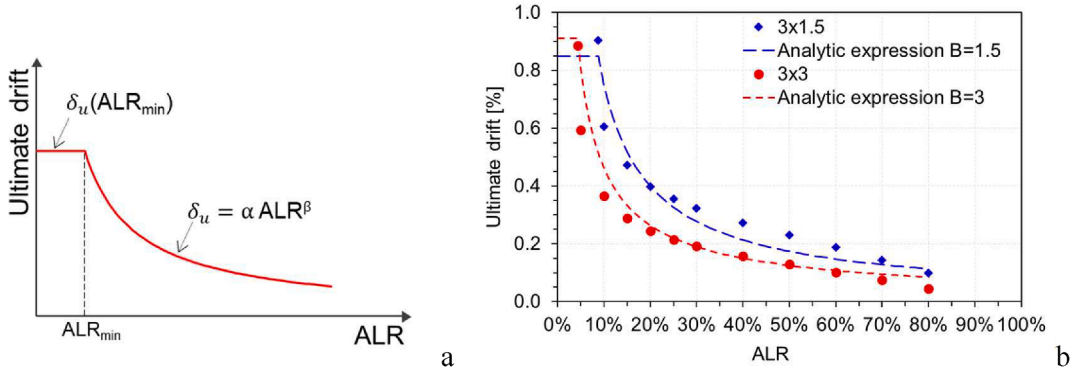

Fig. 11. Analytic expression to predict ultimate drift: (a) theoretical behaviour, and (b) a posteriori verification (CBU material).

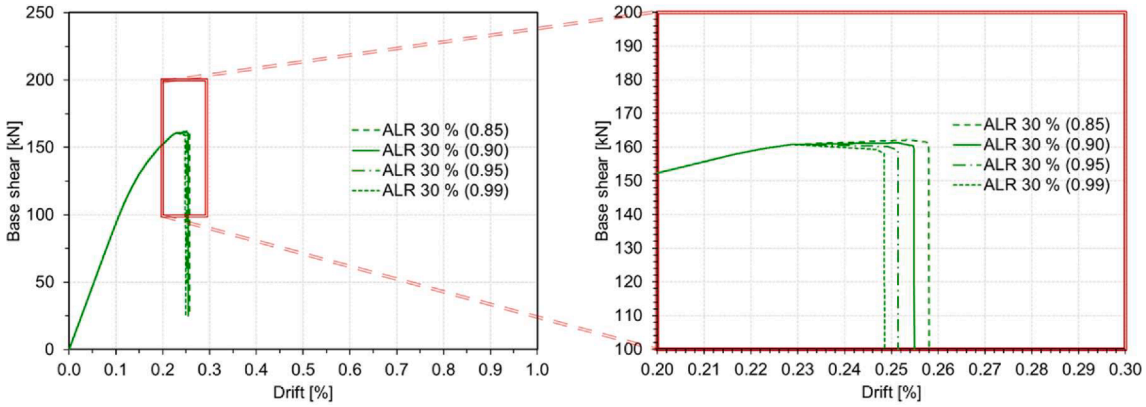

Fig. 12. Influence of damage variable upper limits and the residual stress values on the panel response (material CBU, wall dimensions 3x2 m, ALR 30 %). Base shear-drift curves for cases with damage upper limit equal to 0.85 (with residual stress 15%f_{c0}), 0.90 (with residual stress 10%f_{c0}), 0.95 (with residual stress 5%f_{c0}), and 0.99 (with residual stress 1%f_{c0}).

and $H10$, respectively).

Secondly, the size effect on drift capacity of masonry panels is analysed (Fig. 9b). The size effect on drift capacity has been already observed experimentally (Petry and Beyer, 2014). In particular, Petry & Beyer (Petry and Beyer, 2014) detected a considerable size effect which leads to smaller drift capacities with increasing wall dimensions. Squared panels are considered with a CBU material (Fig. 9b). As can be noted, the ultimate drift shows significant differences between 2x2 and 4x4 walls, being the ultimate drift of the 4x4 systematically and significantly lower than the one of the 2x2 wall for a range of ALR values. Accordingly, a remarkable size effect is observed between the standard walls 2x2 and 4x4, with the same trend observed experimentally. Of course, these two walls have truss elements with the same l_T (and same compressive fracture energy), as the numerical strategy described in Section 2 requires.

To further understand this outcome, a 2x2 wall is scaled uniformly in both directions of a factor 2, so that to obtain a 4x4 wall ("4x4 scaled from 2x2" in Fig. 9b). It should be noted that this "4x4 scaled from 2x2" has truss elements with a double length (and so double compressive fracture energy as the truss mechanical properties have been kept constant) and double truss spacing, and shows ultimate drift values practically coincident with the standard 2x2 wall (Fig. 9a). In addition, a case in which the compressive fracture energy of each truss element has been halved (by adopting a stress–strain curve Fig. 3 with halved area subtended) so that to obtain a consistent value of compressive fracture energy with the standard cases 2x2 and 4x4, named "4x4 scaled from 2x2 (Consistent)", is also shown in Fig. 9b. As can be noted, the ultimate drift values of the "4x4 scaled from 2x2 (Consistent)" result very similar to the 4x4 standard case. Thus, the size effect appears mainly due to the fact that the length of the truss elements l_T is kept constant (so that the compressive fracture energy, which can be seen as a property of the material, remains constant) while the wall dimensions change. This aspect appears reasonable, as in general the localization of the crushing phenomenon does not scale with the wall dimensions, since it can be seen as a constant material property of the masonry type itself (typically close to a height of two blocks). The case "4x4 scaled from 2x2 (Consistent)" also highlights that the truss spacing has a substantially negligible effect on the numerical results, as it was also observed in preliminary analyses (by halving and doubling the truss spacing).

Thirdly, the influence of the wall height H, which modifies of course the wall aspect ratio, is investigated by progressively increasing the height H of the wall, passing from 2 m to 3 and 6 m (Fig. 9c). Lower heights (i.e. aspect ratios lower than 1) are not considered here to guarantee a flexural-dominated failure mode. Passing from a height of 2 m to 3 m, the ultimate drift slightly increases for the range of ALR values considered, while it significantly increases for a height of 6 m. However, if the horizontal displacement is measured at the same height of 2 m ("D2" in Fig. 9c), it can be noted that the aspect ratio has a significantly lower influence on the ultimate drift, almost null for 3x2 D2. On the one hand, top rotation, drift, and bottom rotation mostly coincide for the 2x2 wall. On the other hand, these quantities significantly diverge for the 6x2 wall, suggesting a considerable amount of horizontal displacement due to elastic deformation of the 2D continuum. Accordingly, the influence of the wall height on the ultimate drift appears to be dependent by the way the drift is measured, as with high values of aspect ratios (e.g. 3) the elastic deformation has a significant role. Therefore, only aspect ratios lower than or equal to 2 are considered in the following, as higher values of aspect ratio would need specific considerations on the way the drift has to be measured, which are out of the scope of the present paper. Consequently, with aspect ratios lower than 2 the influence of the wall

height H on the ultimate drift appears negligible (and anyhow included within the uncertainties which characterized the hypotheses of the present model) and it is not considered in the following.

Finally, the influence of the wall width B is investigated numerically on masonry panels with different widths and constant height (Fig. 9d). As highlighted above, the wall height H has a marginal role in the ultimate drift (and some differences are mainly attributable to the elastic bending deflection of the panel when particularly thin). Accordingly, the width of the wall B can be seen as the physical quantity that rules the size effect (Fig. 9b), see Fig. 9d. Indeed, a significant reduction of the ultimate drift for a range of ALR values is observed by passing from a 3x1 wall to 3x2 and 3x3 walls. This is observed also in the case "3x1 D1", i.e. when the horizontal displacement is measured at the height of 1 m so to substantially subtract the elastic bending deflection contribution from the results. Thus, Fig. 9d highlights that the size effect on flexural drift capacity of masonry walls exists, and it is mainly governed by the width of the wall (B).

4. Numerically-based analytic expression for drift capacity

Summing up the outcomes of Section 3, the flexural drift capacity of masonry walls appears significantly influenced by the axial load ratio, the material properties (masonry type), and the size of the panels, directly linked to the width B of the panels. Accordingly, a numerically-based analytic expression (function of ALR, masonry type, and B) is here investigated for the drift capacity of masonry panels. A number of masonry walls with different dimensions (i.e. 1.5x1, 3x2, 6x4, and 12x8 m) and constant aspect ratio (i.e. 1.5) are analysed for the five masonry types described in Section 2.2.1 and for the full range of ALR values (Section 3). The results of the analyses are shown in Fig. 10, in terms of normalized maximum base shear (i.e. maximum numerical base shear normalized to the maximum value of the flexural failure strength domain with 85%f_{c0}) compared with analytical strength domains, and ultimate drift values, which were then used to calibrate the analytic expression.

On the one hand, the normalized maximum base shear results (Fig. 10) highlight a size effect for all masonry types, which becomes significant for ALR values greater than 25%. In particular, decreasing normalized maximum base shear values are obtained while increasing wall dimensions. In Fig. 10, normalized maximum base shear results with ALR lower than $\mathrm{ALR_{min}}$ are also collected to highlight that the numerical results are in good agreement with analytical strength domains, and the size effect for small values of ALR appears negligible. Also in this case, two response types can be observed from the normalized maximum base shear values. Indeed, typical materials in existing masonry structures (CBL, CBU, TUF) show a good agreement with the flexural failure (85%f_{c0}) strength domain with walls characterized by small dimensions (i.e. 1.5x1 and 3x2 m), while larger walls show lower base shear values. Conversely, typical materials in new masonry structures (HCB and CSB) show a good agreement with the flexural failure (85%f_{c0}) strength domain with walls characterized by large dimensions (i.e. 6x4 and 12x8 m), while smaller walls show higher base shear values which becomes rather similar to the flexural failure with 100%f_{c0}. These two response types are mainly due to the higher compressive fracture energy of HCB and CSB with respect the other materials (which can somehow be deduced from Fig. 3 together with l_T).

On the other hand, the size effect is clearly visible on ultimate drift outcomes for all masonry types considered (Fig. 10). Particularly, Fig. 10 highlights that the size effect can be remarkable on the ultimate drift, especially for ALR values around 15%. It should be herein pointed out that the value of $\mathrm{ALR_{min}}$ changes by modifying the wall dimensions, as expected.

Accordingly, given a material type, an analytic expression of the type in Eq. (10) is adopted to fit the ultimate drift values obtained numerically, this time assuming $\alpha(\mathrm{B})$ and $\beta(\mathrm{B})$ functions of the wall width B. Consequently, once one material type is fixed, the functions $\alpha(\mathrm{B})$ and $\beta(\mathrm{B})$ are only function of the wall width B. The functions $\alpha(\mathrm{B})$ and $\beta(\mathrm{B})$ for each material type have been obtained by standard regression on the cases shown in Fig. 10, and a satisfactory match has been found with:

$$\begin{aligned} \alpha &= \alpha_1 \ln(\mathrm{B}) + \alpha_2 \\ \beta &= \beta_1 \mathrm{B}^2 + \beta_2 \mathrm{B} + \beta_3 \end{aligned} \tag{11}$$

Accordingly, the analytic expression for each material type is fully described by the five parameters α_1, α_2, β_1, β_2, and β_3. The resulting parameters for the five material types considered are shown in Table 2.

The proposed numerical strategy does not give information about the ultimate drift for values of ALR lower than $\mathrm{ALR_{min}}$, which is the minimum value of axial load ratio needed to reach compressive failure in a single truss element. A possible suggestion could be to use:

$$\delta_u = \begin{cases} \alpha\ ALR^{\beta} & \text{for} \quad ALR > ALR_{min} \\ \alpha\ ALR_{min}^{\beta} & \text{for} \quad ALR \leqslant ALR_{min} \end{cases} \tag{12}$$

being $\alpha(\mathrm{B})$ and $\beta(\mathrm{B})$ defined in Eq. (11), see e.g. Fig. 11a. Eq. (12) allows to safely define ultimate drift also for values of ALR lower than $\mathrm{ALR_{min}}$, which would be significantly reliant on imperfections and defects of the masonry texture. The predictions of this analytical model are also shown in Fig. 10, and they present a good agreement with the numerical ultimate drift values of all masonry types. ALR values greater than 80% should be not considered as they could lead to masonry panels very close to failure just with vertical loads.

To check the reliability of the numerically-based analytic expression here proposed for drift capacity, an a posteriori verification is conducted on masonry panels which were not used in the regression procedure, e.g. 3x1.5 and 3x3 m walls. An example with the CBU material is shown in Fig. 11b. As it can be observed, the analytical model appears to satisfactorily predict the ultimate drift of masonry walls which were not used in the calibration of the model itself.

5. Conclusions

In this paper, the in-plane flexural drift capacity of masonry walls has been investigated numerically. In particular, a nonlinear truss-based model has been specifically developed to predict the monotonic response of in-plane horizontally-loaded masonry walls undergoing flexural failure. Such numerical strategy, characterized by a band of nonlinear trusses at the wall toe to account for flexural failure, has been conceived with the aim of keeping the mechanical characterization of the model as simple as possible, i.e. the model could be fully described by compressive stress–strain relationships, which can be found in the literature for different masonry types. The modelling strategy has been validated against two pier-scale experimental tests which experienced flexural failure, obtaining promising results.

The numerical strategy resulted also computationally efficient, and this permitted to carry out a comprehensive numerical campaign, predicting the flexural drift capacity of walls with different masonry types and geometrical features, subjected to a full-range of axial load ratios.

As a result, drift capacity has been found to nonlinearly decrease while increasing the axial load ratio, and to be sensibly dependent on the wall width (i.e. the drift capacity diminishes while increasing wall width), for any masonry type. The influence of the wall height on the drift capacity has been found to be mainly due to the elastic deformation of the wall body, and so it mainly depends on the way the drift is measured.

Finally, a simple analytic expression based on a large number of numerical results is deduced for the flexural drift capacity of masonry walls, function of the axial load ratio, masonry type, and wall size. The expression is based on five coefficients which have been obtained by regression for the considered masonry types, and appeared to satisfactorily predict also the ultimate drift of masonry walls which were not used in the calibration of the expression itself. Accordingly, this analytic expression, which can be considered as a surrogate model, could be

implemented in any equivalent frame model used in any commercial code for the analysis of masonry structures to account for a more consistent description of the flexural drift capacity of masonry walls, possibly as function of the axial load ratio, masonry type, and wall size.

The field of application of the modelling strategy herein presented is limited to the investigation of in-plane flexural drift capacity of masonry walls. Future developments could concern simplified numerical models to predict ultimate drift also in case of shear failure modes (e.g. diagonal cracking and sliding).

Declaration of Competing Interest

The authors declare that they have no known competing financial interests or personal relationships that could have appeared to influence the work reported in this paper.

Acknowledgements

The Authors wish to express their acknowledgements to all the partners of the Italian ReLUIS Project - WP10 "Code contributions relating to existing masonry structures" for the productive discussions about the ultimate drift of masonry walls. Mr Stefano Bersani is also acknowledge for his support. This project has received funding from the European Union's Horizon 2020 research and innovation programme under the Marie Sklodowska-Curie grant agreement No 101029792 (HOLAHERIS project, "A holistic structural analysis method for cultural heritage structures conservation").

Appendix A

In this appendix, a parametric investigation on the role of compressive damage variable upper limits and residual stress values in base shear-drift curves of masonry panels is shown and discussed. In particular, Fig. 12 collects the results of a 3x2 m wall (with CBU material and ALR 30 %) where the damage upper limit and the residual stress have been varied in the range $0.85 \div 0.99$ and $15\%f_{c0} \div 1\%f_{c0}$, respectively.

As it can be noted, the results in terms of base shear-drift curves are considerably consistent. Indeed, the variation of ultimate drift by ranging the damage upper limit from 0.85 to 0.99 appears irrelevant and anyway included within the approximations of the regression procedure. Accordingly, the dependence of the panel response on these aspects appears negligible, and compressive damage upper limit and residual stress equal to 0.90 and $10\%f_{c0}$, respectively, are adopted in this paper.

Nevertheless, the load drop which indicates flexural failure arises at very slightly different drift values. In particular, the ultimate drift decreases while the damage upper limit tends to unity (Fig. 12). Indeed, when one or more trusses show compressive damage, the stress is redistributed within the compressed truss elements in the wall toe. Anyway, the damaged truss elements can still provide a residual stress (e.g. $10\%f_{c0}$) and they still have a residual stiffness (e.g. $10\%E_0$), so that they eventually participate in the vertical equilibrium balance, allowing for slightly higher ultimate drifts when adopting higher values of residual stress. In any case, this effect appears negligible for the present research.

References

Abaqus®. Theory manual, Version 6.19, 2019.
Addessi, D., Sacco, E., 2016. Nonlinear analysis of masonry panels using a kinematic enriched plane state formulation. Int. J. Solids Struct. 90, 194–214.
Addessi, D., Di Re, P., Gatta, C., Sacco, E., 2021. Multiscale analysis of out-of-plane masonry elements using different structural models at macro and microscale. Comput. Struct. 247, 106477.
Almeida, F.P., Lourenço, P.B., 2020. Three-dimensional elastic properties of masonry by mechanics of structure gene. Int. J. Solids Struct. 191, 202–211.
Angelillo, M., 2015. Static analysis of a Guastavino helical stair as a layered masonry shell. Compos. Struct. 119, 298–304.
Augenti, N., Parisi, F., 2010. Constitutive models for tuff masonry under uniaxial compression. J. Mater. Civ. Eng. 22 (11), 1102–1111.
Bacigalupo, A., Gambarotta, L., Lepidi, M., 2021. Thermodynamically consistent non-local continualization for masonry-like systems. Int. J. Mech. Sci., 106538
Baraldi, D., Reccia, E., Cecchi, A., 2018. In plane loaded masonry walls: DEM and FEM/DEM models. A critical review. Meccanica 53 (7), 1613–1628.
Benedetti, A., Steli, E., 2008. Analytical models for shear–displacement curves of unreinforced and FRP reinforced masonry panels. Constr. Build. Mater. 22 (3), 175–185.
Bertolesi, E., Milani, G., Lourenço, P., 2016. Implementation and validation of a total displacement non-linear homogenization approach for in-plane loaded masonry. Comput. Struct. 176, 13–33.
Cattari, S., Camilletti, D., D'Altri, A., Lagomarsino, S., 2021. On the use of continuum Finite Element and Equivalent Frame models for the seismic assessment of masonry walls. Journal of Building Engineering 43, 102519.
Cattari, S., Magenes, M., 2021. Benchmarking the software packages to model and assess the seismic response of URM existing buildings through nonlinear analyses. Bull. Earthq. Eng. https://doi.org/10.1007/s10518-021-01078-0.
Cavalagli, N., Cluni, F., Gusella, V., 2013. Evaluation of a statistically equivalent periodic unit cell for a quasi-periodic masonry. Int. J. Solids Struct. 50 (25–26), 4226–4240.
Cavalagli, N., Gusella, V., Severini, L., 2016. Lateral loads carrying capacity and minimum thickness of circular and pointed masonry arches. Int. J. Mech. Sci. 115, 645–656.
Celano, T., Argiento, L.U., Ceroni, F., Casapulla, C., 2021. Literature review of the in-plane behavior of masonry walls: Theoretical vs. experimental results. Materials 14 (11), 3063.
CEN. 1998. European Committee for Standardization. Methods of test for masonry - Part 1. Determination of compressive strength.
CEN. 2002. European Committee for Standardisation (CEN), EN 1052-1: Methods of Test for Masonry – Part 1: Determination of Compressive Strength, Design Code EN 1052-1:1998-12, Brussels, Belgium.
CEN. 2005. European Committee for Standardisation. Eurocode 8: Design of structures for earthquake resistance – Part 3: general rules, seismic actions and rules for buildings, Design Code EN 1998-3, Brussels, Belgium.
Chácara, C., Cannizzaro, F., Pantò, B., Caliò, I., Lourenço, P.B., 2019. Seismic vulnerability of URM structures based on a Discrete Macro-Element Modeling (DMEM) approach. Eng. Struct. 201, 109715.
Chisari, C., Macorini, L., Amadio, C., Izzuddin, B.A., 2018. Identification of mesoscale model parameters for brick-masonry. Int. J. Solids Struct. 146, 224–240.
Clementi, F., Gazzani, V., Poiani, M., Antonio Mezzapelle, P., Lenci, S., 2018. Seismic assessment of a monumental building through nonlinear analyses of a 3D solid model. J. Earthquake Eng. 22 (sup1), 35–61.
Istruzioni per la Valutazione Affidabilistica della Sicurezza Sismica di Edifici Esistenti. Consiglio nazionale delle ricerche, 2014. CNR DT 212/2013.
Commentary, 2019. - Circolare n. 7 del 21 Gennaio 2019, Istruzioni per l'applicazione dell' Aggiornamento delle Norme tecniche per le costruzioni di cui al. DM 17/01/2018.
D'Altri, A.M., Cannizzaro, F., Petracca, M., Talledo, D., 2021. Nonlinear modelling of the seismic response of masonry structures: Calibration strategies. Bull. Earthq. Eng. 1–45.
D'Altri, A., Sarhosis, V., Milani, G., Rots, J., Cattari, S., Lagomarsino, S., Sacco, E., Tralli, A., Castellazzi, G., de Miranda, S., 2020. Modeling strategies for the computational analysis of unreinforced masonry structures: Review and classification. Arch. Comput. Methods Eng. 27, 1153–1185.
De Falco, A., Lucchesi, M., 2007. No tension beam-columns with bounded compressive strength and deformability undergoing eccentric vertical loads. Int. J. Mech. Sci. 49 (1), 54–74.
Di Nino, S., Luongo, A., 2019. A simple homogenized orthotropic model for in-plane analysis of regular masonry walls. Int. J. Solids Struct. 167, 156–169.
Di Nino, S., D'Annibale, F., Luongo, A., 2017. A simple model for damage analysis of a frame-masonry shear-wall system. Int. J. Solids Struct. 129, 119–134.
Dolatshahi, K.M., Nikoukalam, M.T., Beyer, K., 2018. Numerical study on factors that influence the in-plane drift capacity of unreinforced masonry walls. Earthquake Eng. Struct. Dyn. 47 (6), 1440–1459.
Drougkas, A., Verstrynge, E., Hayen, R., Van Balen, K., 2019. The confinement of mortar in masonry under compression: Experimental data and micro-mechanical analysis. Int. J. Solids Struct. 162, 105–120.
Gáspár, O., Sajtos, I., Sipos, A.A., 2021. Friction as a geometric constraint on stereotomy in the minimum thickness analysis of circular and elliptical masonry arches. Int. J. Solids Struct. 225, 111056.
Gatta, C., Addessi, D., Vestroni, F., 2018. Static and dynamic nonlinear response of masonry walls. Int. J. Solids Struct. 155, 291–303.

Jafari, S., Rots, J.G., Esposito, R., 2019. Jafari, S., Rots, J. G., & Esposito, R. (2019). Core testing method to assess nonlinear behavior of brick masonry under compression: A comparative experimental study. Constr. Build. Mater. 218, 193–205.
Jafari, S., Esposito, R., Rots, J.G., 2019. "From brick to element: investigating the mechanical properties of calcium silicate masonry", in *Structural Analysis of Historical Constructions*. Springer, Cham.
Kaushik, H.B., Rai, D.C., Jain, S.K., 2007. Stress-Strain Characteristics of Clay Brick Masonry Under Uniaxial Compression. J. Mater. Civ. Eng. 19 (9), 728–739.
Lagomarsino, S., Penna, A., Galasco, A., Cattari, S., 2013. TREMURI program: An equivalent frame model for the nonlinear seismic analysis of masonry buildings. Eng. Struct. 56, 1787–1799.
Lancioni, G., Lenci, S., Piattoni, Q., Quagliarini, E., 2013. Dynamics and failure mechanisms of ancient masonry churches subjected to seismic actions by using the NSCD method: The case of the medieval church of S. Maria in Portuno. Eng. Struct. 56, 1527–1546.
Lee, J., Fenves, G.L., 1998. Plastic-Damage Model for Cyclic Loading of Concrete Structures. J. Eng. Mech. 124 (8), 892–900. https://doi.org/10.1061/(asce)0733-9399(1998)124:8(892).
Malomo, D., DeJong, M.J., 2021. A Macro-Distinct Element Model (M-DEM) for out-of-plane analysis of unreinforced masonry structures. Eng. Struct. 244, 112754.
Mann, W., Müller, H., 1982. Failure of shear-stressed masonry - an enlarged theory, tests and application to shear walls. Proceedings of the British Ceramic Society.
Messali, F., Rots, J.G., 2018. In-plane drift capacity at near collapse of rocking unreinforced calcium silicate and clay masonry piers. Eng. Struct. 164, 183–194.
Messali, F., Esposito, R., Ravenshorst, G.J.P., Rots, J.G., 2020. Experimental investigation of the in-plane cyclic behaviour of calcium silicate brick masonry walls. Bull. Earthq. Eng. 18 (8), 3963–3994.
Milani, G., Taliercio, A., 2016. Limit analysis of transversally loaded masonry walls using an innovative macroscopic strength criterion. Int. J. Solids Struct. 81, 274–293.
Morandi, P., Albanesi, L., Magenes, G., 2021. In-plane cyclic response of new URM systems with thin web and shell clay units. J. Earthquake Eng. 25 (8), 1533–1564.
Nodargi, N.A., Bisegna, P., 2019. A mixed finite element for the nonlinear analysis of in-plane loaded masonry walls. Int. J. Numer. Meth. Eng. 120 (11), 1227–1248.
Nodargi, N.A., Intrigila, C., Bisegna, P., 2019. Nodargi, N. A., Intrigila, C., & Bisegna, P. (2019). A variational-based fixed-point algorithm for the limit analysis of dry-masonry block structures with non-associative Coulomb friction. Int. J. Mech. Sci. 161, 105078.
Orlando, M., Salvatori, L., Spinelli, P., De Stefano, M., 2016. Displacement capacity of masonry piers: parametric numerical analyses versus international building codes. Bull. Earthq. Eng. 14 (8), 2259–2271.
Petry, S., Beyer, K., 2014. Influence of boundary conditions and size effect on the drift capacity of URM walls. Eng. Struct. 65, 76–88.
Petry, S., Beyer, K., 2015. Force–displacement response of in-plane-loaded URM walls with a dominating flexural mode. Earthquake Eng. Struct. Dyn. 44 (14), 2551–2573.
Petry, S., Beyer, K., 2015. Cyclic test data of six unreinforced masonry walls with different boundary conditions. Earthquake Spectra 31 (4), 2459–2484.
Portioli, F., Casapulla, C., Cascini, L., 2015. An efficient solution procedure for crushing failure in 3D limit analysis of masonry block structures with non-associative frictional joints. Int. J. Solids Struct. 69, 252–266.
Raka, E., Spacone, E., Sepe, V., Camata, G., 2015. Advanced frame element for seismic analysis of masonry structures: model formulation and validation. Earthquake Eng. Struct. Dyn. 44 (14), 2489–2506.
Rezaie, A., Godio, M., Beyer, K., 2020. Experimental investigation of strength, stiffness and drift capacity of rubble stone masonry walls. Constr. Build. Mater. 251, 118972.
Serpieri, R., Albarella, M., Sacco, E., 2017. A 3D Microstructured Cohesive–frictional Interface Model and Its Rational Calibration for the Analysis of Masonry Panels. Int. J. Solids Struct. 122 (123), 110–127.
SIA, 266, 2015. Mauerwerk. Swiss Society of Engineers and Architects (SIA), Zurich.
Smoljanović, H., Živaljić, N., Nikolić, Ž., Munjiza, A., 2018. Numerical analysis of 3D dry-stone masonry structures by combined finite-discrete element method. Int. J. Solids Struct. 137, 150–167.
Technical Norms, 2018. DM 17/01/2018. Norme tecniche per le costruzioni. Ministero delle Infrastrutture. [Technical norms on constructions], Rome, Italy.
Tralli, A., Chiozzi, A., Grillanda, N., Milani, G., 2020. Masonry structures in the presence of foundation settlements and unilateral contact problems. Int. J. Solids Struct. 191, 187–201.
Turnšek, V., Sheppard, P., 1980. The shear and flexural resistance of masonry walls, in *International Research Conference on Earthquake engineering*, Skopje, Japan, 1980.
Turnšek, V., Čačovič, F., 1971. Some experimental results on the strength of brick masonry walls. 2nd International Brick Masonry Conference.
B. Wilding and K. Beyer, "Force-displacement response of in-plane loaded unreinforced brick masonry walls: the Critical Diagonal Crack model," *Bulletin of Earthquake Engineering*, vol. 15, no. 5, 2017.
Wilding, B.V., Beyer, K., 2018. Analytical and empirical models for predicting the drift capacity of modern unreinforced masonry walls. Earthquake Eng. Struct. Dyn. 47 (10), 2012–2031.
Zhang, S., Mousavi, S.M.T., Richart, N., Molinari, J.F., Beyer, 2017. Micro-mechanical finite element modeling of diagonal compression test for historical stone masonry structure. Int. J. Solids Struct. 112, 122–132.